

A matter of time: Using dynamics and theory to uncover mechanisms of transcriptional bursting

Nicholas C Lammers¹, Yang Joon Kim^{1,*}, Jiayi Zhao^{2,*}, Hernan G Garcia^{1,2,3,4,**}

Abstract

Eukaryotic transcription generally occurs in bursts of activity lasting minutes to hours; however, state-of-the-art measurements have revealed that many of the molecular processes that underlie bursting, such as transcription factor binding to DNA, unfold on timescales of seconds. This temporal disconnect lies at the heart of a broader challenge in physical biology of predicting transcriptional outcomes and cellular decision-making from the dynamics of underlying molecular processes. Here, we review how new dynamical information about the processes underlying transcriptional control can be combined with theoretical models that predict not only averaged transcriptional dynamics, but also their variability, to formulate testable hypotheses about the molecular mechanisms underlying transcriptional bursting and control.

Keywords: Live imaging, Transcriptional bursting, Gene regulation, Transcriptional dynamics, Theoretical models of transcription, Non-equilibrium models of transcription, Waiting time distributions

1. A disconnect between transcriptional bursting and its underlying molecular processes

Over the past two decades, new technologies have revealed that transcription is a fundamentally discontinuous process characterized by transient bursts of transcrip-

*These authors contributed equally to this work.

**For correspondence: hggarcia@berkeley.edu (HGG)

¹Biophysics Graduate Group, University of California at Berkeley, Berkeley, California

²Department of Physics, University of California at Berkeley, Berkeley, California

³Department of Molecular and Cell Biology, University of California at Berkeley, Berkeley, California

⁴Institute for Quantitative Biosciences-QB3, University of California at Berkeley, Berkeley, California

tional activity interspersed with periods of quiescence. Although electron microscopy provided early hints of bursty transcription [1], the advent of single-molecule fluorescence *in situ* hybridization (smFISH) [2, 3], was key to establishing its central role in transcription. The single-cell distributions of nascent RNA and cytoplasmic mRNA molecules obtained using this technology provided compelling, if indirect, evidence for the existence and ubiquity of gene expression bursts, and indicated that their dynamics were subject to regulation by transcription factors [4, 5]. These fixed-tissue inferences have been confirmed with new *in vivo* RNA fluorescence labeling technologies such as the MS2/MCP [6] and PP7/PCP systems [7], which directly reveal stochastic bursts of transcriptional activity in living cells in culture and within animals (Figure 1A-C) [8–11].

What is the role of transcriptional bursting in cellular decision-making? One possibility is that bursty gene expression is intrinsically beneficial, helping (for instance) to coordinate gene expression or to facilitate cell-fate decision-making [12]. Alternatively, bursting may not itself be functional, but might instead be a consequence of key underlying transcriptional processes, such as proofreading transcription factor identity [13, 14].

Bursting and its regulation are intimately tied to the molecular mechanisms that underlie transcriptional regulation as a whole. In this Review we argue that, to make progress toward predicting transcriptional outcomes from underlying molecular processes, we can start with the narrower question of how the burst dynamics emerge from the kinetics of molecular transactions at the gene locus. To illustrate the importance and challenge of taking kinetics into account, we highlight two inter-related molecular puzzles that arise from new measurements of the dynamics of key transcriptional processes *in vivo*.

First, as illustrated in Figure 1D and reviewed in detail in Appendix Table A.1, despite qualitatively similar bursty traces from different organisms, bursts unfold across markedly distinct timescales ranging from several minutes [15, 16], to tens of minutes [17, 18], all the way to multiple hours [19]. Is this wide range of bursting timescales across organisms reflective of distinct molecular mechanisms or is it the result of a common set of highly malleable molecular processes?

Second, recent live imaging experiments have revealed a significant temporal disconnect between transcription factor binding events, which generally last for seconds, and the transcriptional bursts that these events control, which may last from a few minutes to multiple hours. The majority of the molecular processes underlying transcriptional control are highly transient (Figure 1E), with timescales ranging from milliseconds to seconds (see Appendix Table A.2 for a detailed tabulation and discussion of these findings).

In this Review, we seek to address this second puzzle by surveying key theoretical and experimental advances that, together, should shed light on the molecular origins of transcriptional bursting and transcriptional regulation. We leverage this framework to examine two kinds of molecular-level models that explain how slow burst dynamics could arise from fast molecular processes. Finally, we present concrete experimental strategies based on measuring variability in the timing of bursts that can be used to discern between molecular models of transcriptional bursting.

Overall, we seek to illustrate how iterative discourse between theory and experiment sharpens our molecular understanding of transcriptional bursting by reformulating cartoon models as concrete mathematical statements. Throughout this Review, we focus on illustrative recent experimental and theoretical efforts; we therefore do not attempt to provide a comprehensive review of the current literature (see [20–25] for excellent reviews).

2. The two-state model: a simple quantitative framework for bursting dynamics

To elucidate the disconnect between molecular timescales and transcriptional bursting, we invoke a simple and widely used model of bursting dynamics: the two-state model of promoter switching. While the molecular reality of bursting is likely more complex than the two-state model suggests [26–28], there is value in examining where this simple model breaks down. This model posits that the promoter can exist in two states: a transcriptionally active ON state and a quiescent OFF state (Figure 2A). The promoter stochastically switches between these states with rates k_{on} and k_{off} , and loads new RNA polymerase II (RNAP) molecules at a rate r when in the ON state [22, 29–31]. Figure 2B shows a hypothetical activity trace for a gene undergoing bursty expression, where a burst corresponds to a period of time during which the promoter is in the ON state. The average burst duration, amplitude and separation are given by $1/k_{\text{off}}$, r and $1/k_{\text{on}}$, respectively.

Because the *instantaneous* transcription initiation rate during a burst is r and zero otherwise, the *average* initiation rate is equal to r times the fraction of time the promoter spends in this ON state p_{on} ,

$$\langle \text{initiation rate} \rangle = r p_{\text{on}}, \quad (1)$$

where brackets indicate time-averaging. As shown in Appendix B, in steady state, p_{on} can be expressed as a function of the transition rates k_{on} and k_{off} :

$$p_{\text{on}} = \frac{k_{\text{on}}}{k_{\text{on}} + k_{\text{off}}}. \quad (2)$$

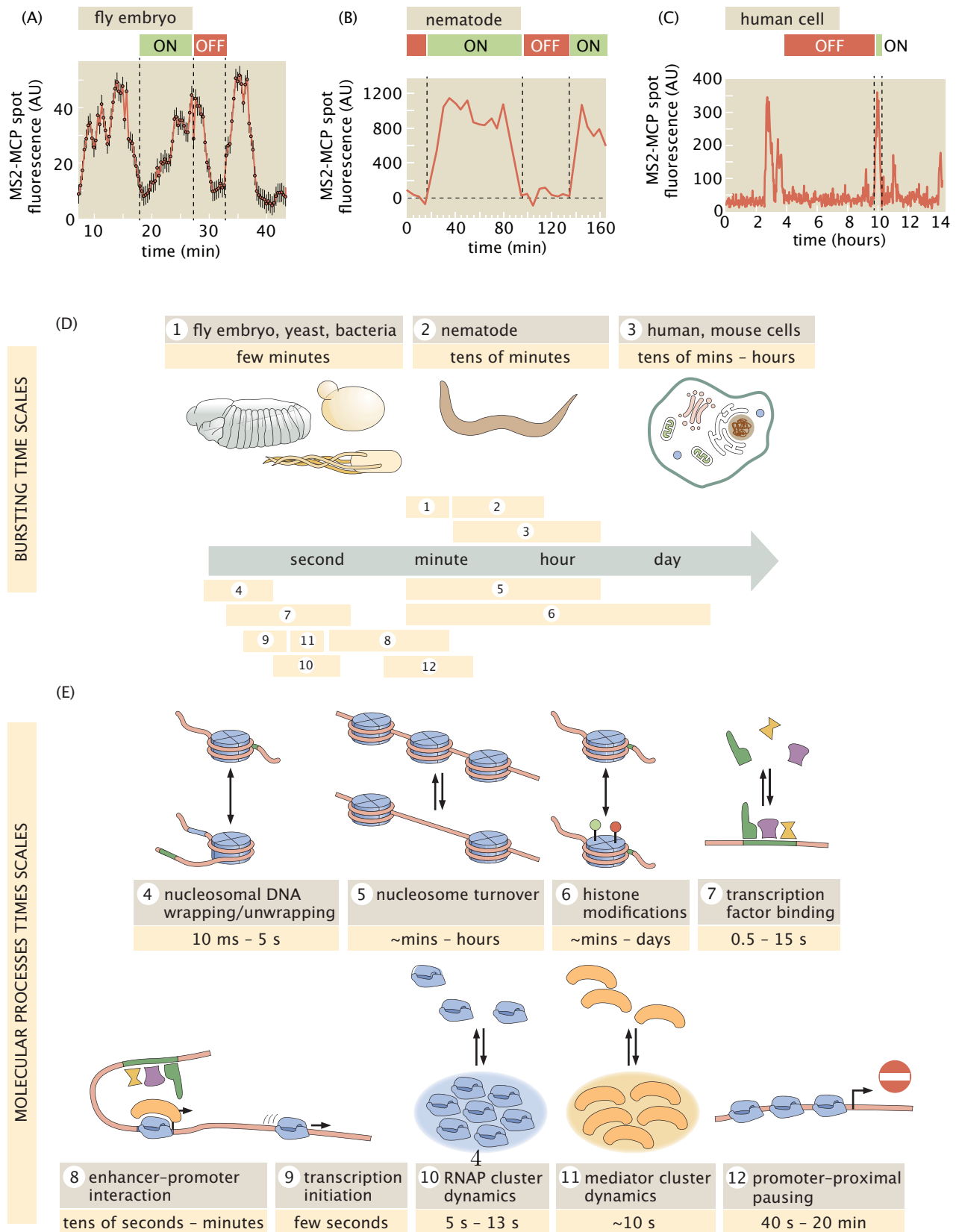


Figure 1: **Separation of timescales between transcriptional bursting and its underlying molecular processes.** See caption in next page.

Figure 1: **Separation of timescales between transcriptional bursting and its underlying molecular processes.** (A,B,C) Transcriptional bursting in (A) an embryo of the fruit fly *Drosophila melanogaster*, (B) the nematode *Caenorhabditis elegans*, and (C) human cells. (D) In these and other organisms, bursting dynamics (average period of ON and OFF) span a wide range of timescales from a few minutes to tens of hours. (E) Timescales of the molecular processes behind transcription range from fast seconds-long transcription factor binding to slower histone modifications, which may unfold across multiple hours or days. A detailed summary of measurements leading to these numbers, including references, is provided in Appendix Table A.1 and Appendix Table A.2. (A, adapted from [16]; B, adapted from [17]; C, adapted from [18]).

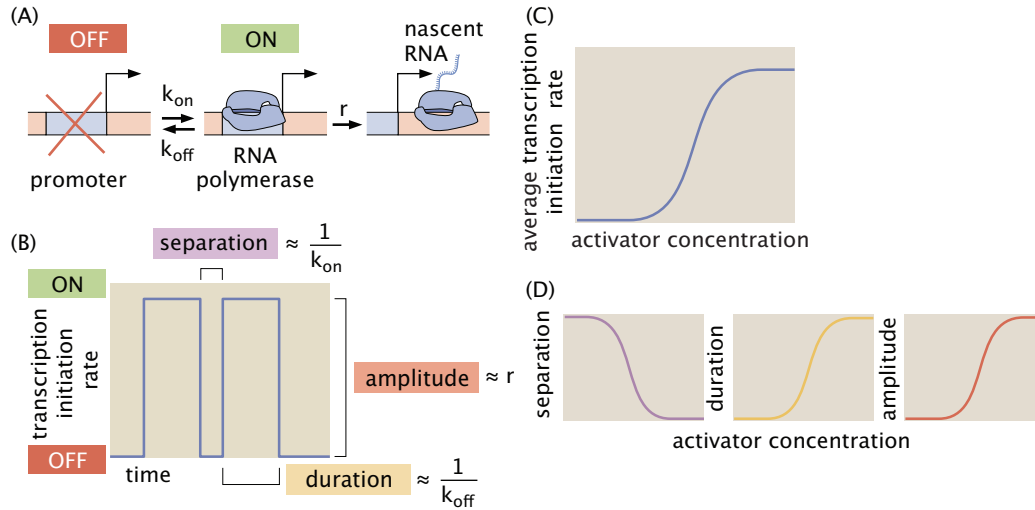


Figure 2: **The two-state model of transcriptional bursting.** (A) A two-state model of transcriptional bursting by a promoter switching between ON and OFF states. (B) Mapping the bursting parameters k_{on} , k_{off} , and r to burst duration, separation, and amplitude, respectively. (C) The action of an activator results in an increase in the average rate of transcription initiation. (D) In the two-state model, this upregulation can be realized by decreasing burst separation, increasing burst duration, increasing burst amplitude, or any combination thereof.

Plugging this solution into Equation 1 results in the average rate of mRNA production as a function of the bursting parameters given by

$$\langle \text{initiation rate} \rangle = \underbrace{r}_{\text{transcription rate in ON state}} \underbrace{\frac{k_{\text{on}}}{k_{\text{on}} + k_{\text{off}}}}_{\text{probability of ON state}}. \quad (3)$$

Equation 3 shows that, within the two-state model, transcription factors can influence the mean transcription rate by modulating any one of the three burst

parameters (or a combination thereof). For example, consider an activator that can increase the mean transcription rate (Figure 2C) by decreasing k_{off} , increasing k_{on} or r , or any combination thereof (Figure 2D). Both live-imaging measurements and smFISH have revealed that the vast majority of transcription factors predominantly modulate burst separation by tuning k_{on} [5, 11, 15, 16, 32–35]. There are also examples of the control of burst amplitude and duration, however [17, 33, 36].

Yet although experiments have identified *which* bursting parameters are under regulatory control, the question of *how* this regulation is realized at the molecular level remains largely open (with a handful of notable exceptions in bacteria [37], yeast [38], and mammalian cell culture [39]). This is because the two-state model is a *phenomenological* model: we can use it to quantify burst dynamics without making any statements about the molecular identity of the burst parameters. Nonetheless, by putting hard numbers to bursting and identifying which parameter(s) are subject to regulation, this framework constitutes a useful quantitative tool to formulate and test hypotheses about the molecular mechanisms underlying transcriptional control.

For instance, consider the observation that many activators modulate burst separation. A simple way to explain this fact is to posit that transitions between the ON and OFF states reflect the binding and unbinding of individual factors to regulatory DNA. Here, k_{off} would be the activator DNA-unbinding rate and k_{on} would be a function of activator concentration $[A]$,

$$k_{\text{on}}([A]) = [A]k_0^b, \quad (4)$$

where k_0^b is the rate constant for activator binding.

A recent study in yeast lent credence to this picture, finding that activator affinity (k^u) might indeed play a role in dictating burst duration [38]. However, for most genes and organisms surveyed so far, the two-state model indicates that transcription factor unbinding alone cannot set the timescale for bursting: if k_{off} were an activator unbinding rate, then it would be on the order of 1 s^{-1} (Figure 1D and E, box 7). Yet, measurements of burst duration reveal that k_{off} must be orders of magnitude smaller ($\lesssim 0.01 \text{ s}^{-1}$, Figure 1D). Thus, the two-state model lends a quantitative edge to the disconnect in Figure 1, reaffirming that transcriptional bursting is unlikely to be solely determined by the binding kinetics of the transcription factors that regulate it. We must therefore extend our simple two-state framework to incorporate molecular mechanisms that allow rapid transcription factor binding and transcriptional bursts that are orders of magnitude slower.

3. Bridging the timescale gap: kinetic traps and rate-limiting steps

Recent works have considered kinetic models of transcription that describe transition dynamics between distinct microscopic transcription factor binding configurations. These models make it possible to investigate how molecular interactions facilitate important behaviors such as combinatorial regulatory logic, sensitivity to changes in transcription factor concentrations, the specificity of interactions between transcription factors and their targets, and transcriptional noise reduction [13, 14, 40–44].

We illustrate how these kinetic models can shed light on the disconnect between the timescales of transcription factor binding and bursting using the activation of the *hunchback* minimal enhancer by Bicoid in the early fruit fly embryo as a case study [34, 40, 43, 45–47]. Recent *in vivo* single-molecule studies have revealed that Bicoid specifically binds DNA in a highly transient fashion ($\sim 1 - 2$ s) [48, 49], suggesting that Bicoid binding cannot dictate the initiation and termination of *hunchback* transcriptional bursts, which happen over minutes [34]. We seek molecular models that recapitulate two key aspects of bursting: (1) the emergence of effective ON and OFF transcriptional states, and (2) “slow” (>1 min) fluctuations between these states. We sketch out the mathematical basis of these efforts and review key results below; more detailed calculations can be found in Appendix C.

Following [40], we consider a simple activation model featuring an enhancer with identical activator binding sites. While the full model for the *hunchback* minimal enhancer consists of six binding sites, we first use a simpler version with three binding sites to introduce key features of our binding model before transitioning to the more realistic six binding sites version when discussing our results. We capture the dynamics of activator binding and unbinding at the enhancer by accounting for the transitions between all possible binding configurations (Figure 3A). Our assumption of identical activator binding sites leads to two simplifications: (1) the same rate, $k_{i,j}$, governs the switching from any configuration with i activators bound to any configuration with j bound and, (2) all binding configurations with the same number n of activators bound have the same rate of transcription, $r_n = r_0 n$, which we posit to be proportional to the number of bound activators. As a result we need not track specific binding configurations and may condense the full molecular representation in Figure 3A into a simpler four-state chain-like model with one state for each possible value of n (Figure 3B).

Transitions up and down the chain in Figure 3B are governed by the effective binding and unbinding rates $k_+(n)$ and $k_-(n)$. To calculate these rates from the microscopic transition rates $k_{i,j}$, consider, for example, that there are three possible ways of transitioning from the 0 state to the 1 state, each with rate $k_{0,1}$. Thus, the

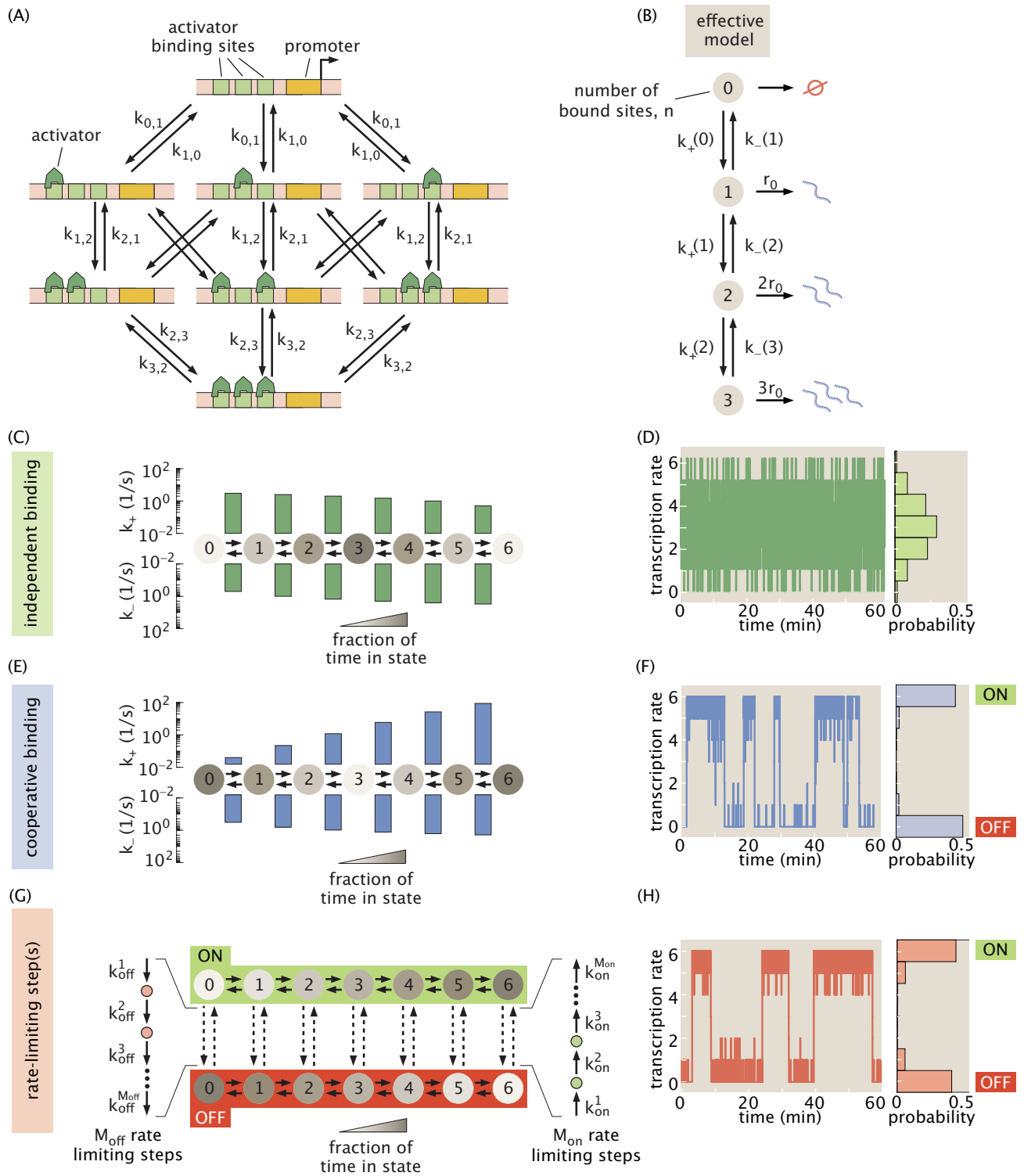


Figure 3: Using theoretical models to understand the origin of ON/OFF bursting dynamic. See caption in the next page.

Figure 3: **Using theoretical models to understand the origin of ON/OFF bursting dynamic.** (A) Model with three activator binding sites. The transition rates between states with i and j activators are given by $k_{i,j}$. (B) The model in (A) can be simplified to an effective four-state chain model in which each state corresponds to a certain number of bound molecules and the transcription rate is proportional to the number of bound activators. (C) Independent activator binding model with effective binding and unbinding rates plotted above and below, respectively. Shading indicates the fraction of time that the system spends in each state. (D) Stochastic simulations indicate that rapid activator binding alone drives fast fluctuations about a single transcription rate. (E) Cooperative binding model in which already-bound activators enhance the binding rate of further molecules. (F) Simulation reveals that cooperativity can cause the system to exhibit bimodal rates of transcription and slow fluctuations between effective ON and OFF states. (G) Rate-limiting step model in which several molecular steps can connect a regime where binding is favored (ON) and a realization where binding is disfavored (OFF). (H) Simulations demonstrate that rate-limiting steps can lead to bimodal transcriptional activity reminiscent of transcriptional bursting. Simulation results were down-sampled to a resolution of 0.5 s to ensure plot clarity in D, F, and H. Scripts used to generate plots in (D), (F), and (H) are available on GitHub [50]. (Parameters: C, D, $k^b = k^u = 0.5 \text{ s}^{-1}$; E, F, $k^b = 0.004 \text{ s}^{-1}$, $k^u = 0.5 \text{ s}^{-1}$; and $\omega = 6.7$; G,H, $k_{on}^u = k_{off}^u = 0.5 \text{ s}^{-1}$, $k_{off}^b = 0.01 \text{ s}^{-1}$, $k_{on}^b = 21 \text{ s}^{-1}$, $M_{off} = 1$, $M_{on} = 2$, $k_{off}^1 = 0.0023$, $k_{on}^1 = k_{on}^2 = 0.0046 \text{ s}^{-1}$.)

effective transition rate between states 0 and 1 is given by $3k_{0,1}$. More generally, in the effective model, activator binding rates are

$$k_+(n) = (N - n)k_{n,n+1}, \quad (5)$$

where n indicates the current number of bound activators and N is the total number of binding sites. Similarly, activator unbinding rates are given by

$$k_-(n) = nk_{n,n-1}. \quad (6)$$

These transition rates allow us to generalize to the more realistic enhancer with six binding sites. We first examine a system in which activator molecules bind and unbind independently from each other (Figure 3C). There are only two unique microscopic rates in this system: activator molecules bind at a rate $k_{i,i+1} = k^b = k_0^b[A]$, with $[A]$ being the activator concentration and k_0^b the binding rate constant, and unbind at a rate $k_{i,i-1} = k^u$. We fix the unbinding rate $k^u = 0.5 \text{ s}^{-1}$ to ensure consistency with recent experimental measurements of Bicoid in [48, 49]. For simplicity, we also set $k^b = 0.5 \text{ s}^{-1}$ (see Appendix C.2.3 for details).

To gain insight into the model's transcriptional dynamics, we employ stochastic simulations based on the Gillespie Algorithm [51]; however a variety of alternative analytic and numerical approaches exist [42, 43, 47]. Our simulations reveal that independent binding leads to a unimodal output behavior in which the transcription

rate fluctuates rapidly about a single average (Figure 3D). This result is robust to our choices of k^b or k^u , as well as the number of binding sites in the enhancer (Appendix C.2.2). The observed lack of slow, bimodal fluctuations leads us to conclude that the independent binding model fails to recapitulate transcriptional bursting.

One way to extend the independent binding model is to allow for cooperative protein-protein interactions between activator molecules [52]. Specifically, we consider a model where bound activator molecules act to catalyze the binding of additional activators. Here, the activator binding rate is increased by a factor ω for every activator already bound, leading to

$$k_{i,i+1} = k^b \omega^i. \quad (7)$$

Because we assume that activator unbinding still occurs independently, the effective unbinding rates remain unchanged (Equation 6).

Stochastic simulations of the cooperative binding model in Figure 3F reveal that the output transcription rate now takes on an all-or-nothing character, fluctuating between high and low values that act as effective ON and OFF states. Further, our simulation indicates that these emergent fluctuations are quite slow (0.13 transitions/min for the system shown), despite fast activator binding kinetics. Both of these phenomena result from large imbalances between $k_+(n)$ and $k_-(n)$ that act as “kinetic traps”.

Consider the case with five bound activators. If $k_+(5) \gg k_-(5)$, then the enhancer is much more likely to bind one more activator molecule and move to state six than to lose an activator and drop to state four. For instance, if $k_+(5)/k_-(5) = 23$ (Figure 3F), then the system will on average oscillate back and forth between states five and six 23 times before it finally passes to state four. While it is possible to generate this kind of trap without cooperativity at one end of the chain or the other by tuning k^b , cooperative interactions are needed to simultaneously achieve traps at both ends.

While we focused on binding-mediated cooperativity here, we note that all results presented above hold equally well for the unbinding-mediated case where cooperative interactions between bound molecules stabilize binding by reducing $k_{i,i-1}$ while maintaining $k_{i,i+1}$ unchanged. As discussed in Appendix C.3.4, our analysis of this unbinding-mediated cooperativity scenario makes the intriguing additional prediction that rapid (~ 1 s) activator dwell times inferred from *in vivo* experiments could mask the existence of rare long-lived (≥ 10 s) binding events that, despite their infrequency, play a key role in driving slow transcriptional burst dynamics. Finally, it is important to note that the phenomenon of emergent slow fluctuations is not limited to activator binding: cooperative interactions in fast molecular reactions elsewhere in

the transcriptional cycle, such as in the dynamics of pre-initiation complex assembly, could, in principle, also induce slow fluctuations.

Inspired by the MWC model of protein allostery [47, 53], a second way to bridge the timescale gap between activator binding and transcriptional bursting is to posit two distinct system configurations: an ON configuration where binding is favored ($k^b \gg k^u$) and an OFF configuration that is less conducive to binding ($k^b \ll k^u$). From any of the seven binding states, this system can transition from OFF to ON by traversing M_{on} slow steps, each with rate $k_{on}^i \ll k^u$, where i is the step number (Figure 3G). Similarly, transitions from ON to OFF are mediated by M_{off} steps with rates given by k_{off}^i . Stochastic simulations indicate that this system yields bimodal transcription that fluctuates between high and low activity regimes on timescales set by the rate-limiting molecular steps (Figure 3H). Thus, as long as these steps induce a sufficiently large shift in activator binding (k^b), the rate-limiting step model reconciles rapid activator binding with transcriptional bursting.

Figure 1B suggests candidates for these slow molecular steps. For example, the ON state in Figure 3G could correspond to an open chromatin state that favors binding while the OFF state could indicate that a nucleosome attenuates binding such that $M_{on} = M_{off} = 1$. Our model also allows multiple distinct rate-limiting steps. For instance, chromatin opening could require multiple histone modifications ($M_{on} \geq 2$, $M_{off} = 1$), or chromatin opening may need to be followed by enhancer-promoter co-localization to achieve a high rate of transcription ($M_{on} = 2$, $M_{off} = 1$).

Although they are not the only possible models, the cooperativity and rate-limiting step scenarios discussed above represent two distinct frameworks for thinking about how slow processes like bursting can coincide with, and even arise from, rapid processes like activator binding. The next challenge in identifying the molecular processes that drive transcriptional bursting is to establish whether these models make experimentally distinguishable predictions.

4. Using bursting dynamics to probe different models of transcription

While we cannot yet directly observe the microscopic reactions responsible for bursting in real time, these processes leave signatures in transcriptional dynamics that may distinguish molecular realizations of bursting such as those of our cooperative binding (Figure 3E) and rate-limiting step (Figure 3G) models. Inspired by [27, 54–56], we examine whether the distribution of observed burst separation times (Figure 4A) distinguishes between these two models. In keeping with literature convention, we refer to these separation times as *first-passage times* from OFF to ON.

The variability in reactivation times provides clues into the number of hidden steps in a molecular pathway. For instance, suppose that bursts are separated by an average time $\tau_{off} = 1/k_{on}$, as defined in the two-state model in Figure 2A and B. If there is only a single rate-limiting molecular step in the reactivation pathway ($M_{on} = 1$ in Figure 3G), then the first-passage times will follow an exponential distribution (Figure 4B) such that the variability, defined as the standard deviation (σ_{off}), will simply be equal to the mean (τ_{off}). Now, consider the case where two distinct molecular steps, each taking an average $\tau_{off}/2$, connect the OFF and ON states ($M_{on} = 2$). To calculate the variability in the time to complete *both* steps and reactivate, we need to add the variability of each step in quadrature:

$$\sigma_{off} = \sqrt{\left(\frac{\tau_{off}}{2}\right)^2 + \left(\frac{\tau_{off}}{2}\right)^2} = \frac{\tau_{off}}{\sqrt{2}}. \quad (8)$$

More generally, in the simple case in which each step has the same rate, given an average first-passage time of τ_{off} , the variability in the distribution of measured first-passage times will decrease as the number of rate-limiting steps, M_{on} , increases following

$$\sigma_{off}(M_{on}) = \frac{\tau_{off}}{\sqrt{M_{on}}}. \quad (9)$$

As predicted by Equation 9, increasing the rate-limiting step number reduces the width of the distribution for the rate-limiting step model obtained from stochastic simulations, shifting passage times from an exponential distribution when $M_{on} = 1$ to increasingly peaked gamma distributions when $M_{on} > 1$ (Figure 4B).

Based on these results, since the fluctuations between high- and low-activity regimes reflect transitions through many individual binding states in the cooperative binding model (Figure 3E), we might also expect this model to exhibit non-exponential first passage times. Instead, the first-passage times are exponentially distributed (Figure 4C). This result is consistent with earlier theoretical work that examined a chain model similar to ours and found that sufficiently large reverse rates (k^u in our case) cause first-passage time distributions to exhibit approximately exponential behavior [57].

The coefficient of variation ($CV = \sigma_{off}/\tau_{off}$) provides a succinct way to summarize the shape of passage time distributions for a wide range of model realizations. Figure 4D plots σ_{off} against τ_{off} for each of the model architectures considered in Figure 4B and C for a range of different τ_{off} values. Points representing distributions with $CV = 1$ will fall on the line with slope one and points for distributions with $CV < 1$ will fall below it. We see that both the cooperative binding model and the single rate-limiting step model have CV values of approximately one for a wide

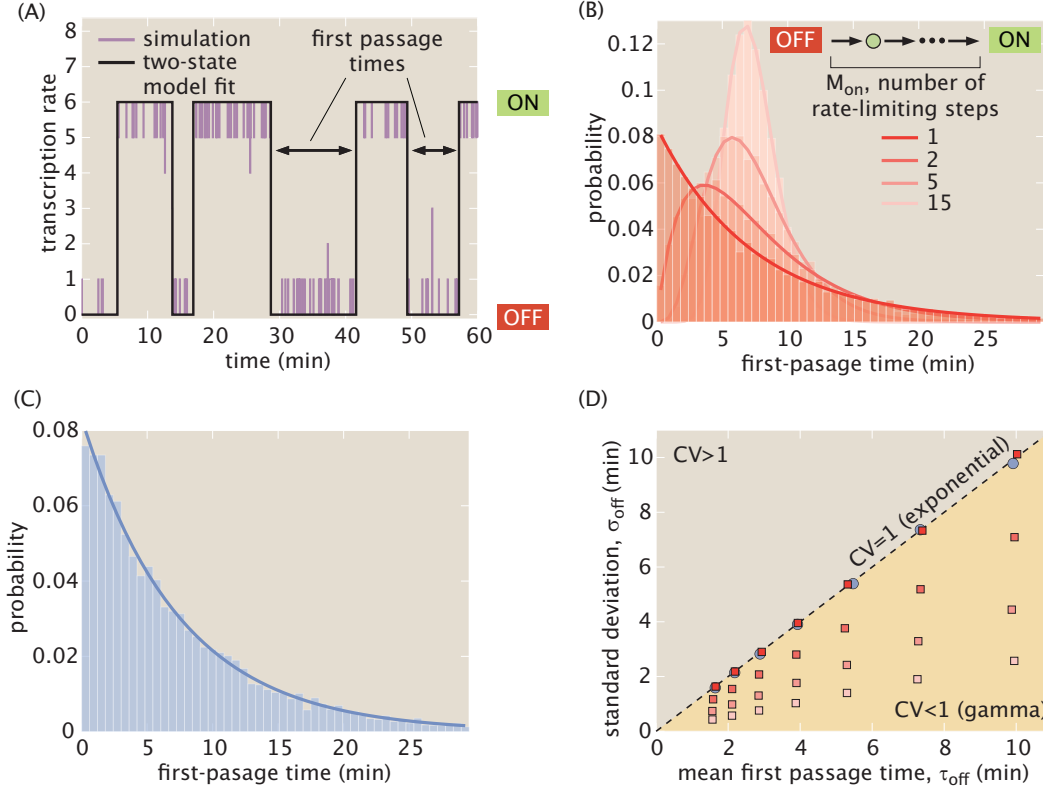


Figure 4: Using first-passage time distributions to discriminate between models of transcriptional bursting. (A) The outcome of stochastic simulations like those in Figure 3D, F, and G (purple) is fit to a two-state model (black) and the first-passage times out of the OFF state are measured. (B) First-passage times for the rate-limiting step model as a function of the number of rate-limiting steps M_{on} calculated using stochastic simulations. A single step results in an exponential distribution, but distributions break from this behavior when more steps are added, yielding increasingly peaked gamma distributions. (C) In contrast, first-passage times for the cooperative binding model follow an exponential distribution. (D) Standard deviation as a function of mean first-passage time for various parameters choices of the cooperative binding (blue) and the rate-limiting step models (red, with color shading indicating the M_{on} values considered in (B)). Distributions with $CV = 1$, such as the exponential distribution, fall on the line of slope one while gamma distributions, with $CV < 1$, fall in the region below this line. Scripts used to generate plots in (A), (B), (C), and (D) are available on GitHub [50]. (Parameters: B, $k_{on}^u = k_{off}^u = 0.5 \text{ s}^{-1}$, $k_{off}^b = 0.01 \text{ s}^{-1}$, $k_{on}^b = 21 \text{ s}^{-1}$, $M_{off} = 1$, $k_{off}^1 = 0.0023 \text{ s}^{-1}$, $k_{on}^i = M_{on} 0.0023 \text{ s}^{-1}$; C, $k^b = 0.004 \text{ s}^{-1}$, $k^u = 0.5 \text{ s}^{-1}$, and $\omega = 6.7$; D (rate-limiting-step model), $k_{on}^u = k_{off}^u = 0.5 \text{ s}^{-1}$, $k_{off}^b = 0.01 \text{ s}^{-1}$, $k_{on}^b = 21 \text{ s}^{-1}$, $M_{off} = 1$, $\tau_{off} \in [1.6, 10.9] \text{ min}$, $k_{off}^1 = 1/\tau_{off} \text{ s}^{-1}$, $k_{on}^i = M_{on}/\tau_{off} \text{ s}^{-1}$; D (cooperativity model), $k^b \in [0.01, 0.003] \text{ s}^{-1}$, $k^u = 0.5 \text{ s}^{-1}$; and $\omega \in [4.5, 7.4]$).

range of τ_{off} values, consistent with exponential behavior. Conversely, all models with multiple rate-limiting steps have slopes that are significantly less than one.

Thus, by moving beyond experimentally measuring average first-passage time for a given gene and examining its *distribution*, it is possible to rule out certain molecular mechanisms. For example, a non-exponential distribution would be evidence against the cooperative binding and single rate-limiting step models (see Appendix C.1 and Appendix C.4 for details about stochastic simulations and first-passage time calculations). While these conclusions are specific to the models considered here, the general approach of invoking the distributions rather than means and using stochastic simulations to derive expectations for different models can be employed to discriminate between molecular hypotheses in a wide variety of contexts. Indeed, the examination of distributions has been revolutionary throughout biology by making it possible to, for example, reveal the nature of mutations [58], uncover mechanisms of control of transcriptional initiation [59] and elongation [60, 61], measure translational dynamics [62], and even count molecules [63].

Note that, while appropriate for *qualitatively* estimating the order of magnitude of bursting timescales, raw fluorescence measurements from MS2 and PP7 experiments such as those in Figure 1A-C do not directly report on the promoter state. Rather, the signal from these experiments is a convolution of the promoter state and the dwell time of each nascent RNA molecule on the gene body [16]. As a result, inference techniques like those developed in [16, 26] are often required to infer underlying burst parameters and promoter states that can be used to estimate first-passage time distributions. Other techniques, such as measuring the short-lived luminescent signal from reporters [27], have also successfully estimated first-passage times.

The first-passage time analyses discussed here are just one of an expansive set of approaches to determining the best model to describe experimental data. For instance, direct fits of models to experimental time traces could be used to identify the most appropriate model (see, e.g. [26, 64]). A discussion of this and other approaches falls beyond the scope of this work, but we direct the reader to several excellent introductions to elements of this field [64–67].

5. Conclusions

The rapid development of live-imaging technologies has opened unprecedented windows into *in vivo* transcriptional dynamics and the kinetics of the underlying molecular processes. We increasingly see that transcription is complex, emergent, and—above all—highly dynamic, but experiments alone still fail to reveal how individual molecular players come together to realize processes that span a wide range of temporal scales, such as transcriptional bursting.

Here we have argued that theoretical models can help bridge this crucial disconnect between single-molecule dynamics and emergent transcriptional dynamics. By committing to mathematical formulations rather than qualitative cartoon models, theoretical models make concrete quantitative predictions that can be used to generate and test hypotheses about the molecular underpinnings of transcriptional control. We have also shown how, although different models of biological phenomena might be indistinguishable in their averaged behavior, these same models often make discernible predictions at the level of the distribution of such behaviors.

Moving forward, it will be critical to continue developing models that are explicit about the kinetics of their constituent molecular pieces, as well as statistical methods for connecting these models to *in vivo* measurements in an iterative dialogue between theory and experiment. In particular, robust model selection frameworks are needed to navigate the enormous space of possible molecular models for transcriptional control. Such theoretical advancements will be key if we are to synthesize the remarkable experimental findings from recent years into a truly mechanistic understanding of how transcriptional control emerges from the joint action of its molecular components.

6. Acknowledgements

We are grateful to Simon Alamos, Lacramioara Bintu, Xavier Darzacq, Jonathan Desponds, Hinrich Boeger, Michael Eisen, Julia Falo-Sanjuan, Anders Hansen, Jane Kondev, Daniel Larson, Tineke Lenstra, Jonathan Liu, Mustafa Mir, Felix Naef, Rob Phillips, Alvaro Sanchez, Brandon Schlomann, Mike Stadler, Meghan Turner and Aleksandra Walczak for useful discussions and comments on the manuscript. However, any errors and omissions are our own. HGG was supported by the Burroughs Wellcome Fund Career Award at the Scientific Interface, the Sloan Research Foundation, the Human Frontiers Science Program, the Searle Scholars Program, the Shurl & Kay Curci Foundation, the Hellman Foundation, the NIH Director’s New Innovator Award (DP2 OD024541-01), and an NSF CAREER Award (1652236).

Appendix A. Literature summary of timescales of transcriptional bursting and associated molecular processes

In this section, we present a survey of timescales observed for transcriptional bursting across a broad swath of organisms (Appendix Table A.1). Further, we review *in vivo* and *in vitro* measurements that have revealed the timescales of the molecular transactions underlying transcription and its control.

Recent technological advances such as single-molecule tracking, live-cell imaging, and a variety of high-throughput sequencing methods, have revealed how eukaryotic transcription is driven by a dizzying array of molecular processes that span a wide range of timescales. The overview of these timescales presented in Figure 1E show how many of these processes are significantly faster than transcriptional bursting.

Chromatin accessibility is a central control point for regulating transcription in eukaryotes [47, 68]. DNA wrapped around nucleosome restricts transcription factor access [68, 69]. Multiple studies have determined the timescales of spontaneous DNA unwrapping and rewinding to be around 0.01-5 s [70–72]. While unwrapping and rewinding are probably too fast to directly lead to long transcriptional bursts, DNA unwrapping might represent a “foothold” by which factors transiently bind DNA and enact larger-scale, sustained chromatin modifications [68].

Interestingly, nucleosome turnover occurs over a longer timescale compatible with bursting, with multiple studies suggesting timescales of several minutes to hours [73–77]. Recent genome-wide studies have measured average nucleosome turnover time to be approximately 1 hour in the fly and in yeast [73, 74]. Further, histone modifications may modulate nucleosomal occupancy [68, 78, 79], and the half-life as well as addition of these modifications can also span a broad range of timescales compatible with bursting, from several minutes to days [80–86].

Once the chromatin is open, enhancers, DNA stretches containing transcription factor binding sites and capable of contacting promoters to control gene expression, become accessible. Transcription factor binding recruits co-factors and general transcription factors to the promoter, triggering the biochemical cascade that ultimately initiates transcription [20]. While the resulting bursts of RNAP initiation last from a few minutes to hours (Figure 1A-D), single-molecule live imaging has shown that transcription factor binding is a highly transient process, with residence times of 0.5-15 s [48, 49, 56, 87–92]. The vast majority of transcription factors bind DNA for seconds, but it is worth noting that some transcription factors and chromatin proteins can bind DNA for minutes [93, 94].

However, the binding of transcription factors, the general transcriptional machinery, and RNAP to the DNA might be more complex than the simple cartoon picture of individual molecules engaging and disengaging from the DNA. For example, recent experiments have revealed that both mediator and RNAP form transient clusters with relatively short

lifetimes in mammalian nuclei of 5-13 s, 10 s, respectively [95–98]. In addition, it is demonstrated that transcription factors can also form clusters *in vivo* [48, 49]. However, how these cluster dynamics relate to transcriptional activity remains unclear.

Further, enhancers and promoters are often separated by kbp to even Mbp. The mechanism by which enhancers find their target loci from such a large distance, and how this contact triggers transcription, remain uncertain and are reviewed in [99]. *In vivo* measurements of enhancer-promoter separation in the *Drosophila* embryo have shown that this distance fluctuates with a timescale of tens of seconds to several minutes [100–102] — timescales strikingly similar to those of bursting. However, recent work has cast doubt on the simple “lock and key” model of enhancer association (stable, direct contact between enhancers and promoters triggers transcription), suggesting instead that enhancers may activate cognate loci from afar and, in some cases, may activate multiple target loci simultaneously [32, 99, 101–105]. Many important questions remain about the nature of enhancer-driven activation and it remains to be seen whether enhancer association dynamics are generic aspect of eukaryotic transcriptional regulation, or whether they only pertain to a subset of organisms and genes.

A single transcriptional burst generally consists of multiple RNAP initiation events (~ 10 -100 at a rate of 1/6-1/3 s when the promoter is ON in *Drosophila*, for instance) [11, 16, 106, 107]. The transcriptional bursting cycle thus encompasses a smaller, faster biochemical cycle in which RNAP molecules are repeatedly loaded and released by the general transcription machinery. One interesting hypothesis for the molecular origin of transcriptional bursting is that the OFF state between bursts is enacted by an RNAP molecule that becomes paused at the promoter, effectively creating a traffic jam [108]. Live imaging and genome-wide studies have shown that RNAP pausing before initiation is common in eukaryotes [108–111] and that its half-life of up to 20 min can be consistent with transcriptional bursting [112–119].

Although the dynamics of some of the molecular processes outlined above are compatible with the long timescales of transcriptional bursting, we still lack a holistic picture of how these kinetics are integrated to realize transcriptional bursts and, ultimately, to facilitate the regulation of gene expression by transcription factors.

We must also acknowledge that we still lie at the very beginning of a reckoning with the dynamics of transcriptional processes as measurements for some molecular processes results in a range of timescales that are difficult to reconcile. In particular, we still lack solid dynamic measurements regarding the assembly of the transcription preinitiation complex. Yet, perhaps more egregious than the lack of any individual dynamical measurement is the lack of a comprehensive, quantitative, and predictive understanding of how these molecular processes interact with one another in time and space to give rise to transcriptional bursting.

Table A.1: **Literature summary of transcriptional bursting.** We attempted to summarize the duration of a single transcriptional burst from various organisms and genes. In the cases where the single-cell data are not available, such as in data stemming from smFISH experiments, we used population averaged T_{ON} and/or T_{OFF} values instead to give a sense on the timescales.

System	Method	Bursting Timescale	Reference
Bacteria			
<i>in vitro</i>	single-molecule assay	5-8 minutes	[37]
<i>Tet</i> system	MS2	$T_{ON} \approx 6$ minutes, $T_{OFF} \approx 37$ minutes	[8]
Fruit fly embryo			
<i>even-skipped</i> stripe 2	MS2	few minutes	[11, 16]
<i>even-skipped</i>	MS2	few minutes	[15]
<i>Notch</i> signaling	MS2	5-20 minutes	[36]
<i>snail</i> , <i>Krüppel</i>	MS2	5 minutes	[32]
gap genes: <i>hunchback</i> , <i>giant</i> , <i>Krüppel</i> , <i>knirps</i>	smFISH	$T_{ON} \approx 3$ minutes, $T_{OFF} \approx 6$ minutes	[33]
<i>hunchback</i>	MS2	few minutes	[34]
<i>even-skipped</i> stripe 2	MS2	few minutes	[11]
Nematode			
<i>Notch</i> signaling	MS2	10-70 minutes	[17]
Human, Mouse			
<i>TGF-β</i> signaling	luciferase assay	few hours	[120]
<i>TFF-1</i> signaling	MS2	few hours	[18]
liver genes	smFISH	$T_{ON} \approx 30$ minutes - 2 hours	[121]
mammalian genes	luciferase assay	few hours	[19]
Amoeba			
actin gene family	RNA-seq	few hours	[122]
actin gene family	MS2	10-15 minutes	[26]

Table A.2: **Summary of measured timescales of underlying molecular processes associated with transcription.**⁵

System	Organism	Experimental method	Timescale	Reference
Nucleosomal DNA Wrapping/Unwrapping				
Mononucleosomes	<i>In vitro</i> reconstitution	FRET	0.1-5 s	[70]
Mononucleosomes	<i>In vitro</i> reconstitution	FRET	10-250 ms	[71]
Mononucleosomes	<i>In vitro</i> reconstitution	Photochemical crosslinking	<1 s	[72]
Nucleosome Turnover				
Histone H3.3	Fruit fly cell	Genome-wide profiling	1-1.5 h	[73]
Histone H3	Yeast	Genomic tiling arrays	~1 h	[74]
Histone H2B, H3, and H4 tagged with GFP	Human cell	FRAP	several minutes	[75]
Histone H1 tagged with GFP	Human cell	FRAP	several minutes	[76]
Histone H3	Plant cell	Isotope labeling	several hours	[77]
Histone Modification				
dCas9 inducible recruitment	Mammalian cell	Single-cell imaging	several hours to days	[80]
rTetR inducible recruitment	Mammalian cell	Single-cell imaging	several hours to days	[81]
Chemical-mediated recruitment	Mammalian cell	Chromatin <i>in vivo</i> assay	several days	[82]
Histone H3	Human cell	Liquid chromatography, mass spectrometer	several hours to days (half-maximal time of methylation)	[83]
Targeted recruitment	Yeast	ChIP	5-8min (reversal of targeted deacetylation) 1.5 min(reversal of targeted acetylation)	[84]
Histone H2a, H2b, H3, and H4	Mammalian cell	Isotope labeling	<15 min (acetylation half-life)	[85]
Histone H2, H2a and H2b	Mammalian cell	Isotope labeling	~3 min (acetylation half-life)	[86]

⁵While the vast majority of transcription factors bind DNA for seconds, it is worth noting that some transcription factors (e.g. TATA-binding protein) and chromatin proteins (e.g. CTCF, Cohesin) can bind DNA for minutes. These outliers are not included in Figure 1.

Transcription Factor Binding				
Bicoid	Fruit fly embryo	SMT	~2 s	[49]
Bicoid	Fruit fly embryo	SMT	~1 s	[48]
Zelda	Fruit fly embryo	SMT	~5 s	[49]
Zelda	Fruit fly embryo	FRAP, FCS	~2-3 s	[56]
Sox2	Mammalian cell	SMT	~12-15 s	[87]
p53	Mammalian cell	SMT	~3.5 s	[88]
p53	Mammalian cell	SMT, FRAP, FCS	~1.8 s	[90]
Glucocorticoid receptor	Mammalian cell	SMT	~8.1 s	[88]
Glucocorticoid receptor	Mammalian cell	SMT	~1.45 s	[89]
STAT1	Mammalian cell	SMT	~0.5 s	[91]
TFIIB	<i>In vitro</i> reconstitution	SMT	~1.5 s	[92]
TATA-binding protein	Mammalian cell	SMT	1.5-2 min	[93]
Chromatin Protein Binding				
CTCF	Mammalian cell	SMT	~1-2 min	[94]
Cohesin	Mammalian cell	SMT	~22 min	[94]
RNAP Cluster Dynamics				
RNAP tagged with Dendra2	Mammalian cell	tcPALM	~12.9 s (with small fraction of stable clusters)	[95]
RNAP tagged with Dendra2	Mammalian cell	tcPALM	~8.1 s	[96]
RNAP tagged with Dendra2	Human cell	Bayesian nanoscopy	several seconds	[97]
RNAP tagged with Dendra2	Human cell	tcPALM	~5.1 s	[98]
Mediator Cluster Dynamics				
Mediator tagged with Dendra2	Mammalian cell	tcPALM	~11.1 s	[95]
Enhancer-Promoter Interaction				
<i>snail</i> shadow enhancer	Fruit fly embryo	MS2, PP7 labeling	~10-40 s (fluctuation cycle interval)	[100]
<i>snail</i> enhancer	Fruit fly embryo	MS2, PP7 labeling	several minutes	[101]
endogenous <i>even-skipped</i> locus with homie insulator	Fruit fly embryo	MS2, PP7 labeling	several minutes	[102]

Transcription Initiation				
<i>even-skipped</i> stripe 2 enhancer	Fruit fly embryo	MS2 labeling	~3 s (promoter ON)	[16]
HIV-1 promoter	Mammalian cell	MS2 labeling	~4.1 s (promoter ON)	[106]
<i>hb</i> P2 enhancer	Fruit fly embryo	MS2 labeling	~6 s	[107]
Promoter-Proximal Pausing				
RNAP tagged with GFP	Human cell	FRAP	~40 s	[112]
RNAP (genome-wide)	Fruit fly cell	RNA sequencing	~2-20 min	[113]
RNAP (genome-wide)	Fruit fly cell	ChIP-nexus	~5-20 min	[114]
RNAP (genome-wide)	Fruit fly cell	Genome-wide footprinting	~2.5-20 min	[115]
RNAP tagged with GFP	Fruit fly salivary glands	Single-cell imaging	~5 min	[116]
RNAP (genome-wide)	Mammalian cell	GRO-seq	~6.9 min (average)	[117]
RNAP (genome-wide)	Fruit fly cell	scRNA-seq	15-20 min (at genes with low activity)	[118]
LacO-tagged minimal CMV promoter	Human cell	MS2 labeling, FRAP	~4 min	[119]

SMT: Single-molecule tracking

FRAP: Fluorescence recovery after photobleaching

FCS: Fluorescence correlation spectroscopy

FRET: Fluorescence resonance energy transfer

ChIP: Chromatin immunoprecipitation

PALM: Photo-activated localization microscopy

Appendix B. Two-state model calculations

As noted in the main text, the average initiation rate is equal to r times the average fraction of time the promoter spends in this ON state p_{on} ,

$$\langle \text{initiation rate} \rangle = r p_{on}. \quad (\text{B.1})$$

To predict the effect of bursting on transcription initiation, it is necessary to determine how p_{on} depends on the bursting parameters. In the mathematical realization of the two-state model shown in Figure 2A, the temporal evolution of p_{off} , the average probability of being in the OFF state, and of p_{on} is given by

$$\frac{dp_{off}}{dt} = -k_{on} p_{off} + k_{off} p_{on}, \quad (\text{B.2})$$

and

$$\frac{dp_{on}}{dt} = k_{on} p_{off} - k_{off} p_{on}. \quad (\text{B.3})$$

To solve these equations, we make the simplifying assumption that our system is in steady state such that these average probabilities of finding the system on the ON and OFF states are constant in time. In this scenario, we can set the rates dp_{off}/dt and dp_{on}/dt to zero. We then solve for k_{off} in terms of k_{on} resulting in

$$k_{off} = \frac{k_{on} p_{off}}{p_{on}}. \quad (\text{B.4})$$

Plugging in the normalization condition $p_{on} + p_{off} = 1$ gives us

$$k_{off} = \frac{k_{on} (1 - p_{on})}{p_{on}}, \quad (\text{B.5})$$

which can be solved in terms of k_{on} , k_{off} , resulting in

$$p_{on} = \frac{k_{on}}{k_{on} + k_{off}}. \quad (\text{B.6})$$

Appendix C. Molecular model calculations

Here we provide a brief overview of the calculations relating to the three theoretical models of transcription presented in Section 3: the independent binding model (Figure 3C), the cooperative binding model (Figure 3E) and the rate-limiting step model (Figure 3G). We also provide resources relating to the calculation of first-passage time distributions discussed in section 4.

Appendix C.1. Stochastic simulations

We make heavy use of stochastic simulations throughout this work. A custom-written implementation of the Gillespie Algorithm [51] was used to simulate trajectories for the various models discussed in the main text. These simulated trajectories were used to generate the activity trace plots in Figure 3D, F, and G, as well as the first-passage time distributions in Figure 4B-D. All code related to this project (including the Gillespie Algorithm implementation for stochastic activity trace generation) can be accessed on GitHub [50].

Appendix C.2. Independent binding model

All calculations in this section pertain to the independent binding model presented in Figure 3C.

Appendix C.2.1. Calculating state probabilities

Calculating the probability of each activity state is central to determining a system's overall transcriptional behavior. Because our mathematical model is a linear chain with no cycles (see Figure 3B), we can make progress towards calculating the steady state probabilities, p_i , by imposing detailed balance, which gives

$$p_n k_+(n) = p_{n+1} k_-(n+1), \quad (\text{C.1})$$

where k_+ and k_- are the effective rates of adding and subtracting a single activator molecule that we define in Figure 3B. Plugging in Equation C.34 and Equation 6 from the main text results in

$$p_n (N - n) k_{n,n+1} = p_{n+1} (n + 1) k_{n+1,n}, \quad (\text{C.2})$$

where, the rates $k_{n,n+1}$ and $k_{n+1,n}$ are the microscopic binding and unbinding rates defined in Figure 3A, respectively. Now we make use of the fact that there are only two unique microscopic rates in the independent binding system: activator molecules bind at a rate $k_{n,n+1} = k^b = k_0^b [A]$, with $[A]$ being the activator concentration and k_0^b the binding rate constant, and unbind at a rate $k_{n,n-1} = k^u$. Plugging these values into Equation C.2 and rearranging leads to

$$p_{n+1} = \left(\frac{N - n}{n + 1} \right) \left(\frac{k^b}{k^u} \right) p_n. \quad (\text{C.3})$$

To further simplify the expression in Equation C.3, we write $\frac{k^u}{k^b}$ as a dissociation constant (K_d), resulting in

$$p_{n+1} = \left(\frac{N - n}{n + 1} \right) \frac{p_n}{K_d}, \quad (\text{C.4})$$

which has the form of a recursive formula for calculating state probabilities from their predecessors. For instance, for the case where $n = 0$ we have

$$p_1 = N \frac{p_0}{K_d}. \quad (\text{C.5})$$

We can extend this logic to calculate the probability of any state, n , as a function of p_0 , leading to

$$p_n = \frac{N!}{(N-n)!n!} \frac{p_0}{K_d^n} = \binom{N}{n} \frac{p_0}{K_d^n}, \quad (\text{C.6})$$

where we have replaced the factorial terms with the binomial coefficient $\binom{N}{n}$ on the far right-hand side can be thought of as accounting for the fact that a given number of activators bound, n , may correspond to multiple microscopic binding configurations (compare Figure 3A and B). Note that $\binom{N}{0} = 1$, which means that Equation C.6 is valid even when $n = 0$. Finally, we impose the normalization condition that the sum of the state probabilities should be equal to 1, which leads to

$$p_n = \frac{p_0 \binom{N}{n} K_d^{-n}}{p_0 \sum_{i=0}^N \binom{N}{i} K_d^{-i}}. \quad (\text{C.7})$$

Canceling out the factors of p_0 gives us our final expression for p_n , namely

$$p_n = \frac{\binom{N}{n} K_d^{-n}}{\sum_{i=0}^N \binom{N}{i} K_d^{-i}} = \frac{\binom{N}{n} K_d^{-n}}{Z}, \quad (\text{C.8})$$

where Z on the far right-hand side indicates the sum of all state weights. Thus, given values of the rates k^b and k^u , which define K_d , we can calculate the probability of the system being in each binding state n . This probability is shown diagrammatically in the shading of the different states in Figure 3C.

Appendix C.2.2. Independent binding cannot produce bimodal transcriptional output

A basic requirement for bimodal transcriptional behavior is that $p_0 > p_1$ and $p_N > p_{N-1}$, where N is the total number of binding sites. Couching this in terms of Equation C.8 leads to

$$\frac{p_0}{p_1} = \frac{1}{N} K_d > 1, \quad (\text{C.9})$$

which simplifies to

$$K_d > N \quad (\text{C.10})$$

for the low activity regime and

$$\frac{p_N}{p_{N-1}} = \frac{1}{N} \frac{1}{K_d} > 1, \quad (\text{C.11})$$

leading to

$$K_d < \frac{1}{N} \quad (\text{C.12})$$

for the high activity regime. Since K_d is set by the ratio $\frac{k^u}{k^b}$, which is constant for all states in the independent binding model, it is not possible for it to be simultaneously larger (Equation C.10) and smaller (Equation C.12) than the number of binding sites N . We thus conclude that independent binding is incompatible with bimodal transcription, regardless of the number of binding sites N .

Appendix C.2.3. Diffusion-limited binding

In the main text we state that we set $k^b = [A]k_0^b$ to 0.5 s^{-1} for the simulations shown in Figure 3C. This is convenient because it leads to a model where half the available sites are bound, on average. This choice is also physically reasonable. Bicoid concentrations in the anterior region of the embryo (where *hunchback* is expressed) are on the order of 30 molecules per μm^3 [45]. A k^b of 0.5 s^{-1} thus implies that $k_0^b \approx 0.017 \mu\text{m}^3\text{s}^{-1}$ per molecule. This falls below a recent estimate for the upper limit on k_0^b for Bicoid binding set by diffusion of $\sim 0.022 \mu\text{m}^3\text{s}^{-1}$ per molecule [44].

We also note here that the largest binding rate in the cooperative binding model (Figure 3E and F), $k^b = 58 \text{ s}^{-1}$, implies a k_0^b that is significantly above diffusion limit diffusion limit for Bicoid estimated in [44]. This high binding rate implies that cooperative binding interactions somehow facilitate the super-diffusive recruitment of additional activator molecules to the gene locus. While speculative, we note that the relatively small energies needed to realized this rapid recruitment in our model (for the plots in Figure 3, the cooperativity factor ω equals 6.7, which corresponds to protein-protein interactions with energies of $1.9k_bT$), suggest that this kind of behavior is at least physically plausible. Alternatively, a significant increase in the concentration of activator molecules in the direct vicinity of the gene locus could facilitate rapid activator binding without exceeding the limits set by diffusion. Recent experiments provide evidence for this kind of local enrichment [49, 56], but it remains to be seen whether this phenomenon plays a role in facilitating gene regulation and, in particular, whether local transcription factor enrichment influences bursting.

Finally, we also note that the rate-limiting step model (Figure 3G and H) assumes a binding rate in the ON state, $k_{on}^b = 21 \text{ s}^{-1}$, that likewise implies a k_0^b that is above Bicoid's likely diffusion limit. This high binding rate was employed primarily

for clarity of exposition, ensuring that the rate-limiting steps separated “ON” and “OFF” activity regimes that were well resolved from one another. Our principal conclusions do not depend on the precise value of k_{on}^b , though, naturally, inferring the durations of OFF (and ON) periods as was done for the waiting time analyses in Figure 4 becomes more difficult. Specifically, smaller values of k_{on}^b reduce the average number of molecules bound when the system is in the ON state,

$$\langle n_{on} \rangle = N \frac{k_{on}^b}{k_{on}^b + k_{on}^u}, \quad (\text{C.13})$$

which leads to more overlap between the transcriptional activity corresponding to the ON and OFF states. It is plausible that a k_{on}^b of this magnitude could be realized by other activator molecules that (i) diffuse faster than Bicoid, (ii) have larger binding target regions, or (iii) are expressed at higher concentrations endogenously. Alternatively, Equation C.13 indicates that a rate-limiting step mechanism that alters the rate of unbinding (k^u) when switching between ON and OFF states instead of, or in conjunction with, k^b could lead to similarly well-resolved ON and OFF states to those in Figure 3H at much lower values of k^b .

Appendix C.3. Cooperative binding

All calculations in this section pertain to the independent binding model presented in Figure 3E.

Appendix C.3.1. Deriving state probabilities with cooperative binding

In Equation 7 of the main text we incorporated cooperativity to binding by adding multiplicative weights, ω , giving

$$k_{i,i+1} = k^b \omega^i. \quad (\text{C.14})$$

This functional form follows from the assumption that each bound activator increases k^b by a constant factor $\omega \geq 1$. This leads the expression for $k_+(n)$

$$k_+^{coop}(n) = (N - n) \omega^n k^b, \quad (\text{C.15})$$

which is a nonlinear function of n . Now, in analogy to the calculations presented in Appendix C.2.1, let’s re-derive our expressions for p_n . To start, we have

$$p_{n+1} = \left(\frac{N - n}{n + 1} \right) \left(\frac{k^b}{k^u} \right) \omega^n p_n. \quad (\text{C.16})$$

Again expressing $\frac{k^u}{k^b}$ as a dissociation constant (K_d), we obtain

$$p_{n+1} = \left(\frac{N-n}{n+1} \right) \frac{\omega^n p_n}{K_d}. \quad (\text{C.17})$$

We can also extend this logic to calculate the probability of any state, n , as a function of p_0 , leading to

$$p_n = \frac{N!}{(N-n)!n!} \frac{\omega^{\frac{n(n-1)}{2}} p_0}{K_d^n} = \binom{N}{n} \frac{\omega^{\frac{n(n-1)}{2}} p_0}{K_d^n}. \quad (\text{C.18})$$

Finally, by requiring that all state probabilities sum to one, we obtain

$$p_n = \frac{\binom{N}{n} \omega^{\frac{n(n-1)}{2}} K_d^{-n}}{Z}, \quad (\text{C.19})$$

where Z again denotes the sum of all state weights as in Equation C.8. We have used these expressions to calculate the probability of each state shown using the shading in Figure 3E.

Appendix C.3.2. Cooperativity permits bimodal expression

Now, let's use Equation C.18 to examine how the addition of the cooperativity factor ω makes bimodal bursting possible. Recall that bimodal gene expression requires that $p_0 > p_1$ and $p_N > p_{N-1}$. For the low activity regime, cooperativity is not relevant because there are no already bound activators, and so the form of the requirement remains the same, namely

$$\frac{p_0}{p_1} = \frac{1}{N} K_d > 1. \quad (\text{C.20})$$

However, things change in the high activity regime. Here, we have

$$\frac{p_N}{p_{N-1}} = \frac{1}{N} \frac{\omega^{N-1}}{K_d} > 1. \quad (\text{C.21})$$

In stark contrast to the independent binding case, we see that the addition of ω makes it possible to realize both conditions simultaneously, opening the door to bimodal burst behaviors. Specifically, bimodality demands

$$K_d > N, \quad (\text{C.22})$$

and

$$\omega > (N K_d)^{\frac{1}{N-1}} \quad (\text{C.23})$$

to be true.

These requirements thus demonstrate that cooperativity is required to achieve bimodal bursting in the context of this binding model. Indeed, the cooperative binding system shown in Figure 3E and F meets these criteria, having $K_d = 116$ and $\omega = 6.7$, both of which are comfortably above the lower bounds described above for a system with six binding sites ($N = 6$).

Appendix C.3.3. Cooperativity is necessary to simultaneously achieve kinetic trapping at both ends of the chain

In the main text we introduced the concept of “kinetic trapping”; a phenomenon in which large imbalances between $k_+(n)$ and $k_-(n)$ cause a system to get trapped in high and low activity states for periods of time that far exceed the timescale of individual binding/unbinding events. Here, we show that cooperativity ($\omega > 1$) is needed in order to achieve this kind of trapping at *both* the high and low ends of the binding chain shown in Figure 3B simultaneously.

To begin, we note that the relations $k_-(1) > k_+(1)$ and $k_-(N-1) < k_+(N-1)$ are necessary to have traps at the low and high ends of the chain, respectively. Thus both conditions must hold simultaneously for traps to exist at the low and high ends simultaneously. We can use Equation C.15 and Equation 6 to express these requirements in terms of system parameters. For the low activity regime, we have

$$\frac{k_-(1)}{k_+(1)} = \frac{K_d}{(N-1)\omega} > 1, \quad (\text{C.24})$$

and for the higher regime we obtain

$$\frac{k_+(N-1)}{k_-(N-1)} = \frac{\omega^{N-1}}{(N-1)K_d} > 1. \quad (\text{C.25})$$

We can simplify these requirements to obtain upper and lower bounds on ω , namely

$$\left[K_d(N-1) \right]^{\frac{1}{N-1}} < \omega < \frac{K_d}{N-1}. \quad (\text{C.26})$$

We see that Equation C.26 implies restrictions on the relationship between K_d and N . Specifically, there must be a gap between the upper and lower bounds in Equation C.26 such that there exist viable ω values. This means that

$$\left[K_d(N-1) \right]^{\frac{1}{N-1}} < \frac{K_d}{N-1}, \quad (\text{C.27})$$

must hold. Upon simplification, this gives

$$(N - 1)^N < K_d^{N-2}. \quad (\text{C.28})$$

$$(N - 1)^2 < K_d. \quad (\text{C.29})$$

Equation C.29 tells us that the dissociation constant must be larger than one (indeed, it must be larger than 25 for an $N = 6$ binding site system). This implies that the expression for the lower ω bound on the left-hand side of Equation C.26 is guaranteed to be greater than one as well because

$$K_d(N - 1) > 1, \quad (\text{C.30})$$

and therefore

$$1 < \left[K_d(N - 1) \right]^{\frac{1}{N-1}} < \omega. \quad (\text{C.31})$$

This indicates that cooperative interactions are necessary to realize kinetic traps on both ends of the chain, though it hints at the fact that increasing the number of binding sites, N , should enable trapping with lower values of ω .

Appendix C.3.4. Off rate-mediated cooperativity can also generate transcriptional bursting

It is straight-forward to adapt our discussion of on rate-mediated cooperativity to capture the case where cooperative interactions act instead to stabilize bound factors and thereby reduce the effective off rate. Indeed, the expressions are identical save for the fact that the basal binding rate is *divided* by powers of ω , rather than multiplied. Namely,

$$k_{i,i-1} = \frac{k^u}{\omega^i}. \quad (\text{C.32})$$

This leads the expression for $k_-(n)$

$$k_-^{coop}(n) = n \frac{k^u}{\omega^n}. \quad (\text{C.33})$$

Since activator binding is assumed to be independent, the expression for $k_+(n)$ is identical to that for the independent binding model, namely,

$$k_+(n) = (N - n)k_{n,n+1}. \quad (\text{C.34})$$

These expressions lead to a model wherein the unbinding rate decreases significantly as more and more activators become bound (Figure C.5A). From this point

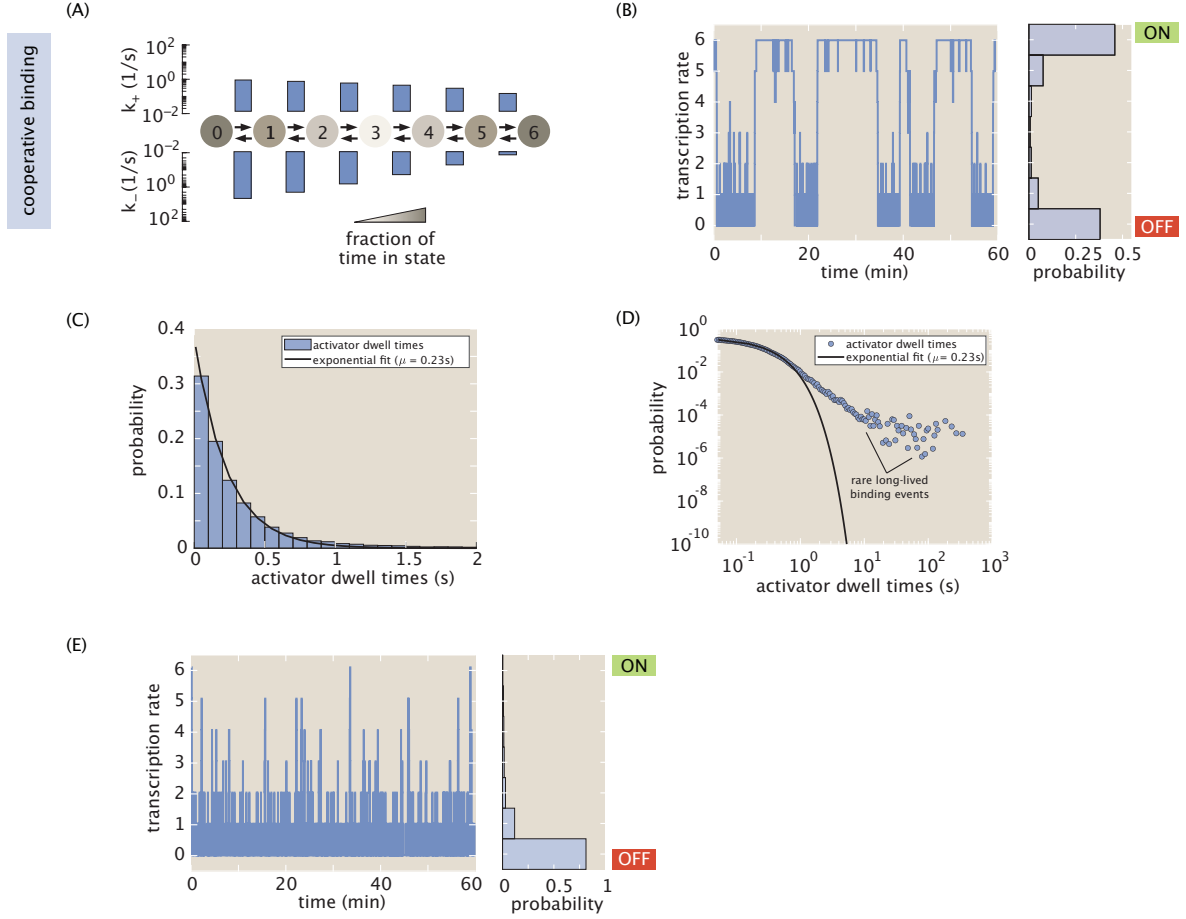


Figure C.5: **Cooperative binding model with off rate-mediated cooperativity.** (A) Cooperative binding model in which stabilizing interactions between bound activators decreases the unbinding rate. (B) Simulation reveals that off rate-mediated cooperativity can cause the system to exhibit bimodal rates of transcription and slow fluctuations between effective ON and OFF states that are comparable to those observed for on rate-mediated cooperativity (Figure 3E and F). (C) The predicted distribution of unbinding times is well fit by a single exponential, despite the presence of cooperative interactions. (D) However, this fit masks the presence of rare long-lived binding events that are signatures of the cooperative effects that enable slow timescale bursting. These events can be seen as a significant deviation between the empirical distribution of dwell times (blue circles) from the exponential fit when we shift to looking at the data on a log-log scale. (E) To examine the role these long-lived events play in bursting, we conducted simulations in which all activator dwell events were capped to a maximum duration of 10 seconds; i.e. we forced all activators still bound after 10 seconds to unbind. These simulations revealed that removing long-lived binding events abolishes all burst-like activity.

forward, the expressions for state probabilities (starting with Equation C.16) have precisely the same form as those for the on rate-mediated case.

With the off rate-mediated model thus defined, we are in a position to once again employ stochastic simulations to explore the impact of cooperativity on transcriptional dynamics. These reveal that stabilizing cooperative interactions amongst bound activator molecules can also generate slow bimodal transcriptional fluctuations (Figure C.5B). While this is perhaps not surprising given the close mathematical parallels between the on and off rate-mediated cooperativity models, this result emphasizes the breadth of potential molecular mechanisms that could lead to transcriptional bursting.

Given these results, it is interesting to ask whether stabilizing cooperative interactions should have a clear signature in experimental measurements of individual activator residence times. Somewhat surprisingly, a distribution of single particle unbinding events generated via stochastic simulations are well described by a single exponential fit with a mean residence time of 0.23 s^{-1} (Figure C.5C), which is on the same scale as the empirical measurements in [49]. Yet, this is no the full story. A close inspection of the distribution of dwell times reveals a small ($\lesssim 5\%$) fraction of very long lived binding events that last for 10s to 100s of seconds (Figure C.5D).

Such events might very well be missed in an *in vivo* experiment due either to how rare they are or to limitations on observation time imposed by the bleaching of fluorescent proteins. To examine the role these events play in dictating burst dynamics, we conducted simulations invoking parameters identical to those used to generate the trace shown in Figure C.5B, with one important alteration: all activators still bound after 10 seconds were forced to unbind. This effectively capped the activator dwell time at 10 seconds, thereby abolishing all long-lived binding events. Figure C.5E shows the result of this exercise, clearly indicating, that removing rare long-lived binding events abolishes burst-like dynamics. These results thus indicate that hard-to-detect long-lived binding events could play a key role in generating slow burst dynamics, suggesting that it could be of interest to design experiments explicitly aimed at searching for long-lived binding events *in vivo*. In closing, we note that similar results relating to activator dwell time distributions in the presence of cooperative interactions are discussed in [44]. We direct readers to this work for an excellent, detailed discussion on this topic.

Appendix C.4. First-passage time calculations

In this review we used stochastic simulations (briefly outlined in Appendix C.1) to arrive at expectations for the form of first-passage time distributions for the cooperative binding and rate-limiting step models. All relevant scripts are available at

[GitHub](#). We also note that the functional forms for waiting time distributions can be calculated using analytical methods such as Laplace Transforms. We do not provide the details for this approach here, but point the reader to [57, 123], as well as the sources cited therein, for more information.

References

1. McKnight, S. L. & Miller, O. L. Post-replicative nonribosomal transcription units in *D. melanogaster* embryos. *Cell* **17**, 551–563 (1979).
2. Femino, A. M., Fay, F. S., Fogarty, K. & Singer, R. H. Visualization of Single RNA Transcripts in Situ. *Science* **280**, 585–590 (1998).
3. Raj, A., van den Bogaard, P., Rifkin, S. A., van Oudenaarden, A. & Tyagi, S. Imaging individual mRNA molecules using multiple singly labeled probes. *Nature Methods* **5**, 877–879 (2008).
4. Raj, A. & van Oudenaarden, A. Single-Molecule Approaches to Stochastic Gene Expression. *Annual Review of Biophysics* **38**, 255–270 (2009).
5. Xu, H., Sepúlveda, L. A., Figard, L., Sokac, A. M. & Golding, I. Combining protein and mRNA quantification to decipher transcriptional regulation. *Nature Methods* **12**, 739–742 (2015).
6. Bertrand, E. *et al.* Localization of ASH1 mRNA particles in living yeast. *Mol Cell* **2**, 437–445 (1998).
7. Chao, J. A., Patskovsky, Y., Almo, S. C. & Singer, R. H. Structural basis for the coevolution of a viral RNA-protein complex. *Nature Structural and Molecular Biology* **15**, 103–105 (2008).
8. Golding, I., Paulsson, J., Zawilski, S. M. & Cox, E. C. Real-time kinetics of gene activity in individual bacteria. *Cell* **123**, 1025–1036 (2005).
9. Chubb, J. R., Trecek, T., Shenoy, S. M. & Singer, R. H. Transcriptional Pulsing of a Developmental Gene. *Current Biology* **16**, 1018–1025 (2006).
10. Larson, D. R., Zenklusen, D., Wu, B., Chao, J. A. & Singer, R. H. Real-Time Observation of Transcription Initiation and Elongation on an Endogenous Yeast Gene. *Science* **332**, 475–478 (2011).
11. Bothma, J. P. *et al.* Dynamic regulation of eve stripe 2 expression reveals transcriptional bursts in living *Drosophila* embryos. *Proceedings of the National Academy of Sciences* **111**, 10598–10603 (2014).

12. Eldar, A. & Elowitz, M. B. Functional roles for noise in genetic circuits. *Nature* **467**, 167–173 (2010).
13. Grah, R., Zoller, B. & Tkačik, G. Normative models of enhancer function. *bioRxiv*, 2020.04.08.029405 (2020).
14. Shelansky, R. & Boeger, H. Nucleosomal proofreading of activator–promoter interactions. *Proceedings of the National Academy of Sciences of the United States of America* **117**, 2456–2461 (2020).
15. Berrocal, A., Lammers, N., Garcia, H. G. & Eisen, M. B. Kinetic sculpting of the seven stripes of the *Drosophila* even-skipped gene. *bioRxiv*, 335901 (2020).
16. Lammers, N. C. *et al.* Multimodal transcriptional control of pattern formation in embryonic development. *Proceedings of the National Academy of Sciences of the United States of America* **117**, 836–847 (2020).
17. Lee, C. H., Shin, H. & Kimble, J. Dynamics of Notch-dependent transcriptional bursting in its native context. *Developmental Cell* **50**, 426–435.e4 (2019).
18. Rodriguez, J. *et al.* Intrinsic Dynamics of a human gene reveal the basis of expression heterogeneity. *Cell* **176**, 213–226.e18 (2019).
19. Suter, D. M. *et al.* Mammalian genes are transcribed with widely different bursting kinetics. *Science* **332**, 472–474 (2011).
20. Coulon, A., Chow, C. C., Singer, R. H. & Larson, D. R. Eukaryotic transcriptional dynamics: From single molecules to cell populations. *Nature Reviews Genetics* **14**, 572–584 (2013).
21. Lenstra, T. L., Rodriguez, J., Chen, H. & Larson, D. R. Transcription Dynamics in Living Cells. *Annual Review of Biophysics* **45**, 25–47 (2016).
22. Wang, Y., Ni, T., Wang, W. & Liu, F. Gene transcription in bursting: a unified mode for realizing accuracy and stochasticity. *Biological Reviews* **94**, 248–258 (2019).
23. Rodriguez, J., Larson, D. R. & ARjatscls, L. Transcription in Living Cells: Molecular Mechanisms of Bursting. *Annual Review of Biochemistry*, 1–24 (2020).
24. Wong, F. & Gunawardena, J. Gene Regulation in and out of Equilibrium. *Annual Review of Biophysics* **49**, 199–226 (2020).
25. Phillips, R. *et al.* Figure 1 Theory Meets Figure 2 Experiments in the Study of Gene Expression. *Annu. Rev. Biophys* **48**, 121–163 (2019).
26. Corrigan, A. M., Tunnacliffe, E., Cannon, D. & Chubb, J. R. A continuum model of transcriptional bursting. *eLife* **5**, e13051 (2016).

27. Zoller, B., Nicolas, D., Molina, N. & Naef, F. Structure of silent transcription intervals and noise characteristics of mammalian genes. *Mol Syst Biol* **11** (2015).
28. Morrison, M., Razo-Mejia, M. & Phillips, R. Reconciling Kinetic and Equilibrium Models of Bacterial Transcription. *bioRxiv*, 2020.06.13.150292 (2020).
29. Sanchez, A. & Golding, I. Genetic determinants and cellular constraints in noisy gene expression. *Science* **342**, 1188–1193 (2013).
30. Boeger, H., Shelansky, R., Patel, H. & Brown, C. R. From structural variation of gene molecules to chromatin dynamics and transcriptional bursting. *Genes* **6**, 469–483 (2015).
31. Munsky, B., Fox, Z. & Neuert, G. Integrating single-molecule experiments and discrete stochastic models to understand heterogeneous gene transcription dynamics. *Methods* **85**, 12–21 (2015).
32. Fukaya, T., Lim, B. & Levine, M. Enhancer control of transcriptional bursting. *Cell* **166**, 358–368 (2016).
33. Zoller, B., Little, S. C. & Gregor, T. Diverse spatial expression patterns emerge from unified kinetics of transcriptional bursting. *Cell* **175**, 835–847.e25 (2018).
34. Desponds, J. *et al.* Precision of readout at the hunchback gene: analyzing short transcription time traces in living fly embryos. *PLOS Computational Biology* **12** (2016).
35. Lionnet, T. *et al.* A transgenic mouse for in vivo detection of endogenous labeled mRNA. *Nature Methods* **8**, 165–170 (2011).
36. Falo-Sanjuan, J., Lammers, N. C., Garcia, H. G. & Bray, S. J. Enhancer priming enables fast and sustained transcriptional responses to Notch signaling. *Developmental Cell* **50**, 411–425 (2019).
37. Chong, S., Chen, C., Ge, H. & Xie, X. S. Mechanism of transcriptional bursting in bacteria. *Cell* **158**, 314–326 (2014).
38. Donovan, B. T. *et al.* Live-cell imaging reveals the interplay between transcription factors, nucleosomes, and bursting. *The EMBO Journal* (2019).
39. Nicolas, D., Phillips, N. E. & Naef, F. What shapes eukaryotic transcriptional bursting? *Molecular BioSystems* **13**, 1280–1290 (2017).
40. Tran, H. *et al.* Precision in a rush: Trade-offs between reproducibility and steepness of the hunchback expression pattern. *PLoS Computational Biology* **14**, e1006513 (2018).

41. Li, C., Cesbron, F., Oehler, M., Brunner, M. & Höfer, T. Frequency Modulation of Transcriptional Bursting Enables Sensitive and Rapid Gene Regulation. *Cell Systems* **6**, 409–423 (2018).
42. Scholes, C., Depace, A. H. & Lvaro Sá Nchez, A. ´. Math j Bio Combinatorial Gene Regulation through Kinetic Control of the Transcription Cycle. *Cell Systems* **4**, 97–108 (2017).
43. Estrada, J., Wong, F., DePace, A. & Gunawardena, J. Information Integration and Energy Expenditure in Gene Regulation. *Cell* **166**, 234–44 (2016).
44. Desponds, J., Vergassola, M. & Walczak, A. M. A mechanism for hunchback promoters to readout morphogenetic positional information in less than a minute. *eLife* **9**, e49758 (2020).
45. Gregor, T., Tank, D. W., Wieschaus, E. F. & Bialek, W. Probing the limits to positional information. *Cell* **130**, 153–164 (2007).
46. Park, J. *et al.* Dissecting the sharp response of a canonical developmental enhancer reveals multiple sources of cooperativity. *eLife* **8**, e41266 (2019).
47. Eck, E. *et al.* Quantitative dissection of transcription in development yields evidence for transcription factor-driven chromatin accessibility. *bioRxiv*, 2020.01.27.922054 (2020).
48. Mir, M. *et al.* Dense bicoid hubs accentuate binding along the morphogen gradient. *Genes and Development* **31**, 1784–1794 (2017).
49. Mir, M. *et al.* Dynamic multifactor hubs interact transiently with sites of active transcription in drosophila embryos. *eLife* **7**, 1–27 (2018).
50. Lammers, N. C., Kim, Y. J., Zhao, J. & Garcia, H. G. *Code from “A matter of time: Using dynamics and theory to uncover mechanisms of transcriptional bursting”* 2020.
51. Gillespie, D. T. Exact stochastic simulation of coupled chemical reactions. *Journal of Physical Chemistry* **81**, 2340–2361 (1977).
52. Uzman, A. Genes and signals: Ptashne, M., Gann, A. *Biochemistry and Molecular Biology Education* **30**, 340–341 (2002).
53. Marzen, S., Garcia, H. G. & Phillips, R. Statistical mechanics of Monod-Wyman-Changeux (MWC) models. *Journal of Molecular Biology* **425**, 1433–1460 (2013).
54. Yildiz, A., Tomishige, M., Vale, R. D. & Selvin, P. R. Kinesin Walks Hand-Over-Hand. *Science* **303**, 676–678 (2004).

55. Suter, D. M., Molina, N., Naef, F. & Schibler, U. Origins and consequences of transcriptional discontinuity. *Current Opinion in Cell Biology* **23**, 657–662 (2011).
56. Dufourt, J. *et al.* Temporal control of gene expression by the pioneer factor Zelda through transient interactions in hubs. *Nature Communications* **9** (2018).
57. Bel, G., Munsky, B. & Nemenman, I. The simplicity of completion time distributions for common complex biochemical processes. *Physical Biology* **7** (2010).
58. Luria, S. E. & Delbrück, M. Mutations of bacteria from virus sensitivity to virus resistance. *Genetics* **28** (1943).
59. Sanchez, A., Garcia, H. G., Jones, D., Phillips, R. & Kondev, J. Effect of promoter architecture on the cell-to-cell variability in gene expression. *PLoS Computational Biology* **7** (2011).
60. Serov, A. S., Levine, A. J. & Mani, M. Abortive Initiation as a Bottleneck for Transcription in the Early Drosophila Embryo. *arXiv*, 1701.06079 (2017).
61. Ali, M. Z., Choubey, S., Das, D. & Brewster, R. C. Probing Mechanisms of Transcription Elongation Through Cell-to-Cell Variability of RNA Polymerase. *Biophysical Journal* **118**, 1769–1781 (2020).
62. Cai, L., Friedman, N. & Xie, X. S. Stochastic protein expression in individual cells at the single molecule level. *Nature* **440**, 358–362 (2006).
63. Rosenfeld, N., Young, J. W., Alon, U., Swain, P. S. & Elowitz, M. B. Gene regulation at the single-cell level. *Science* **307**, 1962–1965 (2005).
64. Silk, D., Kirk, P. D., Barnes, C. P., Toni, T. & Stumpf, M. P. Model Selection in Systems Biology Depends on Experimental Design. *PLoS Computational Biology* **10**, 1003650 (2014).
65. Sivia, D. S. & Skilling, J. *Data Analysis - A Bayesian Tutorial* 2nd (Oxford University Press, 2006).
66. Mehta, P. *et al.* A high-bias, low-variance introduction to Machine Learning for physicists. *arXiv*, 1803.08823v3 (2019).
67. Devilbiss, F. & Ramkrishna, D. Addressing the Need for a Model Selection Framework in Systems Biology Using Information Theory. *Proceedings of the IEEE* **105**, 330–339 (2017).
68. Bowman, G. D. & Poirier, M. G. Post-translational modifications of histones that influence nucleosome dynamics. *Chemical Reviews* **115**, 2274–2295 (2015).

69. Kouzarides, T. Chromatin modifications and their function. *Cell* **128**, 693–705 (2007).
70. Tomschik, M., Zheng, H., Van Holde, K., Zlatanova, J. & Leuba, S. H. Fast long-range, reversible conformational fluctuations in nucleosomes revealed by single-pair fluorescence resonance energy transfer. *Proceedings of the National Academy of Sciences of the United States of America* **102**, 3278–3283 (2005).
71. Li, G., Levitus, M., Bustamante, C. & Widom, J. Rapid spontaneous accessibility of nucleosomal DNA. *Nature Structural and Molecular Biology* **12**, 46–53 (2005).
72. Kassabov, S. R., Zhang, B., Persinger, J. & Bartholomew, B. SWI/SNF unwraps, slides, and rewaps the nucleosome. *Molecular Cell* **11**, 391–403 (2003).
73. Deal, R. B., Henikoff, J. G. & Henikoff, S. Genome-wide kinetics of nucleosome turnover determined by metabolic labeling of histones. *Science* **328**, 1161–1165 (2010).
74. Ghuysen, J. M. *et al.* Dynamics of replication-independent Histone turnover in budding yeast. *Science* **315**, 1405–1409 (2007).
75. Kimura, H. & Cook, P. R. Kinetics of core histones in living human cells: Little exchange of H3 and H4 and some rapid exchange of H2B. *Journal of Cell Biology* **153**, 1341–1353 (2001).
76. Misteli, T., Gunjan, A., Hock, R., Bustin, M. & Brown, D. T. Dynamic binding of histone H1 to chromatin in living cells. *Nature* **408**, 877–881 (2000).
77. Waterborg, J. H. Histone synthesis and turnover in alfalfa. Fast loss of highly acetylated replacement histone variant H3.2. *Journal of Biological Chemistry* **268**, 4912–4917 (1993).
78. Ludwig, C. H. & Bintu, L. Mapping chromatin modifications at the single cell level. *Development* **146** (2019).
79. Lawrence, M., Daujat, S. & Schneider, R. Lateral thinking: How Histone modifications regulate gene expression. *Trends in Genetics* **32**, 42–56 (2016).
80. Braun, S. M. *et al.* Rapid and reversible epigenome editing by endogenous chromatin regulators. *Nature Communications* **8** (2017).
81. Bintu, L. *et al.* Dynamics of epigenetic regulation at the single-cell level. *Science* **351**, 720–724 (2016).
82. Hathaway, N. A. *et al.* Dynamics and memory of heterochromatin in living cells. *Cell* **149**, 1447–1460 (2012).

83. Zee, B. M. *et al.* In vivo residue-specific histone methylation dynamics. *Journal of Biological Chemistry* **285**, 3341–3350 (2010).
84. Katan-Khaykovich, Y. & Struhl, K. Dynamics of global histone acetylation and deacetylation in vivo: Rapid restoration of normal histone acetylation status upon removal of activators and repressors. *Genes and Development* **16**, 743–752 (2002).
85. Chestier, A. & Yaniv, M. Rapid turnover of acetyl groups in the four core histones of simian virus 40 minichromosomes. *Proceedings of the National Academy of Sciences of the United States of America* **76**, 46–50 (1979).
86. Jackson, V., Shires, A., Chalkley, R. & Granner, D. K. Studies on highly metabolically active acetylation and phosphorylation of histones. *Journal of Biological Chemistry* **250**, 4856–4863 (1975).
87. Chen, J. *et al.* Single-molecule dynamics of enhanceosome assembly in embryonic stem cells. *Cell* **156**, 1274–1285 (2014).
88. Morisaki, T., Müller, W. G., Golob, N., Mazza, D. & McNally, J. G. Single-molecule analysis of transcription factor binding at transcription sites in live cells. *Nature Communications* **5** (2014).
89. Gebhardt, J. C. M. *et al.* Single-molecule imaging of transcription factor binding to DNA in live mammalian cells. *Nature Methods* **10** (2013).
90. Mazza, D., Abernathy, A., Golob, N., Morisaki, T. & McNally, J. G. A benchmark for chromatin binding measurements in live cells. *Nucleic Acids Research* **40** (2012).
91. Speil, J. *et al.* Activated STAT1 transcription factors conduct distinct saltatory movements in the cell nucleus. *Biophysical Journal* **101**, 2592–2600 (2011).
92. Zhang, Z. *et al.* Rapid dynamics of general transcription factor TFIIB binding during preinitiation complex assembly revealed by single-molecule analysis. *Genes & development* **30**, 2106–2118 (2016).
93. Teves, S. S. *et al.* A stable mode of bookmarking by TBP recruits RNA polymerase II to mitotic chromosomes. *eLife* **7**, e35621 (2018).
94. Hansen, A. S., Pustova, I., Cattoglio, C., Tjian, R. & Darzacq, X. CTCF and cohesin regulate chromatin loop stability with distinct dynamics. *eLife* **6**, e25776 (2017).
95. Cho, W. K. *et al.* Mediator and RNA polymerase II clusters associate in transcription-dependent condensates. *Science* **361**, 412–415 (2018).

96. Cho, W.-K. *et al.* RNA Polymerase II cluster dynamics predict mRNA output in living cells. *eLife* **5**, e13617 (2016).
97. Chen, X. *et al.* Study of RNA Polymerase II clustering inside live-cell nuclei using Bayesian Nanoscopy. *ACS Nano* **10**, 2447–2454 (2016).
98. Cisse, I. I. *et al.* Real-time dynamics of RNA polymerase II clustering in live human cells. *Science* **341**, 664–667 (2013).
99. Furlong, E. E. & Levine, M. Developmental enhancers and chromosome topology. *Science* **361**, 1341–1345 (2018).
100. Heist, T., Fukaya, T. & Levine, M. Large distances separate coregulated genes in living *Drosophila* embryos. *Proceedings of the National Academy of Sciences of the United States of America* **116**, 15062–15067 (2019).
101. Lim, B., Heist, T., Levine, M. & Fukaya, T. Visualization of transvection in living *Drosophila* embryos. *Molecular Cell* **70**, 287–296.e6 (2018).
102. Chen, H. *et al.* Dynamic interplay between enhancer–promoter topology and gene activity. *Nature Genetics* **50**, 1296–1303 (2018).
103. Gu, B. *et al.* Transcription-coupled changes in nuclear mobility of mammalian cis-regulatory elements. *Science* **359**, 1050–1055 (2018).
104. Benabdallah, N. S. *et al.* Decreased enhancer–promoter proximity accompanying enhancer activation. *Molecular Cell* **76**, 473–484.e7 (2019).
105. Schoenfelder, S. & Fraser, P. Long-range enhancer–promoter contacts in gene expression control. *Nature Reviews Genetics* **20**, 437–455 (2019).
106. Tantale, K. *et al.* A single-molecule view of transcription reveals convoys of RNA polymerases and multi-scale bursting. *Nature Communications* **7**, 12248 (2016).
107. Garcia, H. G., Tikhonov, M., Lin, A. & Gregor, T. Quantitative imaging of transcription in living *Drosophila* embryos links polymerase activity to patterning. *Current Biology* **23**, 2140–2145 (2013).
108. Jonkers, I. & Lis, J. T. Getting up to speed with transcription elongation by RNA polymerase II. *Nature Reviews Molecular Cell Biology* **16**, 167–177 (2015).
109. Bartman, C. R. *et al.* Transcriptional burst initiation and Polymerase pause release are key control points of transcriptional regulation. *Molecular Cell* **73**, 519–532.e4 (2019).

110. Gaertner, B. & Zeitlinger, J. RNA polymerase II pausing during development. *Development* **141**, 1179–1183 (2014).
111. Core, L. J., Waterfall, J. J. & Lis, J. T. Nascent RNA sequencing reveals widespread pausing and divergent initiation at human promoters. *Science* **322**, 1845–1848 (2008).
112. Steurer, B. *et al.* Live-cell analysis of endogenous GFP-RPB1 uncovers rapid turnover of initiating and promoter-paused RNA Polymerase II. *Proceedings of the National Academy of Sciences of the United States of America* **115**, E4368–E4376 (2018).
113. Henriques, T. *et al.* Widespread transcriptional pausing and elongation control at enhancers. *Genes & Development* **32**, 26–41 (2018).
114. Shao, W. & Zeitlinger, J. Paused RNA Polymerase II inhibits new transcriptional initiation. *Nature Genetics* **49**, 1045–1051 (2017).
115. Krebs, A. R. *et al.* Genome-wide single-molecule footprinting reveals high RNA Polymerase II turnover at paused promoters. *Molecular Cell* **67**, 411–422.e4 (2017).
116. Buckley, M. S., Kwak, H., Zipfel, W. R. & Lis, J. T. Kinetics of promoter Pol II on Hsp70 reveal stable pausing and key insights into its regulation. *Genes & Development* **28**, 14–19 (2014).
117. Jonkers, I., Kwak, H. & Lis, J. T. Genome-wide dynamics of Pol II elongation and its interplay with promoter proximal pausing, chromatin, and exons. *eLife* **3**, e02407 (2014).
118. Henriques, T. *et al.* Stable pausing by RNA Polymerase II provides an opportunity to target and integrate regulatory signals. *Molecular Cell* **52**, 517–528 (2013).
119. Darzacq, X. *et al.* In vivo dynamics of RNA Polymerase II transcription. *Nature Structural and Molecular Biology* **14**, 796–806 (2007).
120. Molina, N. *et al.* Stimulus-induced modulation of transcriptional bursting in a single mammalian gene. *Proceedings of the National Academy of Sciences of the United States of America* **110**, 20563–20568 (2013).
121. Halpern, K. B. Bursty gene expression in the intact mammalian liver. *Molecular Cell* **58**, 147–156 (2015).

122. Tunnacliffe, E., Corrigan, A. M. & Chubb, J. R. Promoter-mediated diversification of transcriptional bursting dynamics following gene duplication. *Proceedings of the National Academy of Sciences of the United States of America* **115**, 8364–8369 (2018).
123. Schnitzer, M. J. & Block, S. M. Statistical kinetics of processive enzymes. *Cold Spring Harbor Symposia on Quantitative Biology* **60**, 793–802 (1995).